Asian Journal of Physics Vol 15, No. 4, (2006) 283-293

Counterpropagating beams in photorefractive crystals and optically induced photonic lattices

M Belic[1], M Petrovic[2], D Jovic[2], A Strinic[2], D Arsenovic[2], S Prvanovic[2] and N Petrovic[1]
[1]*Texas A & M University at Qatar, P O Box 5825, Doha, Qatar*
[2]*Institute of Physics, P O Box 57, 11001 Belgrade, Serbia*

A comprehensive numerical study of counterpropagating incoherent beams in isotropic photorefractive crystals and optically induced photonic lattices in such crystals is carried out. A local model with saturable Kerr-like nonlinearity is adopted for the photorefractive media, with an optically generated two-dimensional photonic lattice written within the crystal. Different head-on incident beam structures are considered, such as Gaussians, dipoles, and vortices. We review some of our earlier work and present novel results on the dynamical behavior of counterpropagating beams in a finite hexagonal photonic lattice.

1 Introduction

Self-trapped beams of light propagating without change in a diffractive nonlinear medium, better known as spatial solitons, have become much investigated objects in nonlinear optics [1-3]. Of considerable importance in all-optical information processing, they come in a variety of forms – as bullets, screening, quadratic, photovoltaic, and lattice solitons, or as bright, dark, and grey [2]. They are generated in different media and by different nonlinear mechanisms, but the self-focusing effect, produced by light-induced changes in the medium's index of refraction, appears as the common thread in all mechanisms. Self-focusing in photorefractive (PR) crystals is achieved through the generation of the space charge field, which is caused by the photo-induced redistribution of charges that modifies the index of refraction. Application of an external DC electric field across the crystal and an additional uniform illumination turn out to be necessary for a more effective soliton formation process.

An additional interest in the propagation and interactions of self-focused light is generated when photonic lattices are imbedded in PR crystals, giving rise to the discrete diffraction and offering intriguing waveguiding possibilities [3]. Periodic two-dimensional (2D) arrays of optically induced waveguides allowed for the observation of novel self-trapped optical structures – the so-called discrete or lattice solitons, including the discrete vortex solitons [4]. Of special concern are the modes connected with a defect embedded in a perfect infinite or finite lattice [5]. An especially interesting geometry from the applications point of view is the photonic crystal fiber (PCF), in which a finite hexagonal lattice of holes is infused into a silica fiber, with the central hole absent [6]. Such a 2D PCF with a central defect, also referred to as the "holey fiber", offers a different scenario of waveguiding from the perfectly periodic infinite PC with dielectric rods in that it displays huge refractive index step, that the light is pinned to the defect, and that no photonic band gap is needed to support the localized 2D solitonic waves.

So far the formation and interactions of spatial solitons and vortices have been studied mostly in the copropagation geometry, with a few exceptions [7-11]. In these references the counterpropagating (CP) solitons were considered theoretically in one transverse dimension (1D), in Kerr and local PR media, and in the steady state. Nowhere in the literature could we find a reference to CP lattice solitons or vortices. In Refs. [12-14] we studied numerically 2D CP vector solitons and displayed some novel dynamical beam structures in PR crystals. Some of those results are reproduced here. In addition, we introduce 2D CP lattice solitons and vortices, and present some of their interesting features.

Also, we compare our numerical simulations with the experimental evidence of 2D CP vector solitons

and other self-trapped optical structures in PR crystals [15-17], and present the splitup transition and dynamical instabilities of such structures. We consider the propagation of various CP beam structures in PR crystals, such as the dipole-dipole and vortex-vortex beam arrangements [18]. To validate our numerical algorithm and compare it with our linear stability analysis (LSA) [17], we utilize broader hyper-Gaussian beams in numerical simulations, in order to display ordinary modulational instabilities (MI) and pattern formation of CP beams [19], in contraposition to the splitup transition. Concerning CP lattice solitons, we display stable transverse splitup transitions of different kinds, as well as dynamical symmetry-broken splitup transitions, where no definitive patterns are visible. We demonstrate that CP vortices generally break up into filaments that are pinned at or in-between lattice sites, but also that their stability can be enhanced in the presence of lattice beams.

2 The model

To understand the behavior of CP vector solitons we formulated a time-dependent model for the formation of self-trapped CP optical beams [12], based on the theory of PR effect. The model consists of wave equations in the paraxial approximation for the propagation of CP beams and a relaxation equation for the generation of the space charge field in the PR crystal, in the isotropic approximation. The model equations in the computational space are of the form:

$$i\partial_z F = -\Delta F + \Gamma E F\,, \qquad -i\partial_z B = -\Delta B + \Gamma E B\,, \tag{1}$$

$$\tau\partial_t E + E = -\frac{I}{1+I}\,, \tag{2}$$

where F and B are the forward and the backward propagating beam envelopes, Δ is the transverse Laplacian, is the dimensionless coupling constant, and E the homogenous part of the space charge field. The relaxation time of the crystal τ also depends on the total intensity, $\tau = \tau_0/(1+I)$. The quantity $I = |F|^2+|B|^2$ is the laser light intensity, measured in units of the background intensity. A scaling $x/x_0 \to x$, $y/x_0 \to y$, $z/L_D \to z$, is utilized in writing the propagation equations, where x_0 is the typical FWHM beam waist and L_D is the diffraction length. The assumption, appropriate to the experimental conditions utilized, is that the incoherent counterpropagating components interact only through the intensity-dependent space charge field. To make matters simple, we did not account for the temperature (diffusion) effects, although they are found to influence the interaction of CP beams [10]. In the experiment [15-17] these effects were compensated by focusing the input B beam at the place of the exit and in the direction of the output F beam. When the propagation in photonic lattices is considered, Eq. (2) is modified, to include the transverse intensity distribution of the optically induced lattice array I_g:

$$\tau\partial_t E + E = -\frac{I+I_g}{1+I+I_g}\,, \tag{2a}$$

For the lattice array we choose a fixed hexagonal arrangement of beams, with variable intensities, and with the central beam absent. Such an arrangement is reminiscent of the holey fibers [6], except that there are no holes here. Instead, the laser beams modulate the index of refraction. They are assumed to be degenerate and incoherent with the forward and backward components, and of higher intensity. We also assume that the array beams are far enough from each other, so that the interaction between them is negligible, and that the influence of the CP beams on the lattice beams can be neglected.

The propagation equations are solved numerically, concurrently with the temporal equations, in the manner described in Ref. [15] and references cited therein. The dynamics is such that the space charge field

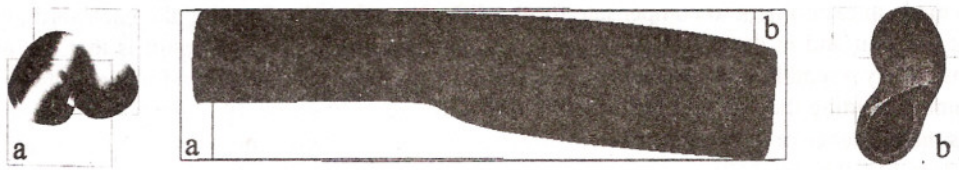

Fig. 1. Isosurface plots of a CP soliton after the splitup transition. Forward propagating component is displayed in the steady state, (a) View along the entrance face of the crystal, (b) View along the exit face of the crystal. Simulation parameters: $|F_0|^2=|B_L|^2 = 0.6$, $\Gamma = 7.17$, $L= 5.75L_D= 23$ μm, and initial beam widths (FWHM) are 20 μm.

builds up towards the steady state, which depends on the light distribution, which in turn is slaved to the change in the space charge field. As it is seen, this simple type of dynamics does not preclude a more complicated dynamical behavior. Some of our numerical results are presented concurrently with the experimental results in Figs. 1-3. It is seen that the numerics agree, at least qualitatively, with the experiment.

A more difficult problem is to provide an explanation of the nature and the cause of the transverse splitup instability. In Refs. [12, 13] we presented a simple theory of beam displacement – derived in two independent ways – that can account for such transverse shifts. In Refs. [16, 17] we attempted to utilize the standard theory of MI to obtain a threshold curve for the CP beams splitup that at least qualitatively agrees with the experimental and numerical results. In doing so, we were aware of the fact that, although both are symmetry breaking phenomena, the pattern forming MI represents a spontaneous breaking of the translational symmetry of a homogeneous state, whereas the splitup transition is the breaking of the rotational symmetry of an isolated CP soliton. Thus, MI involves the appearance of transverse waves at a critical value of k_c, whereas the splitup instability involves a jump of the peaked structure in the transverse inverse space for some value of k_c. The two values of k_c might, but need not be connected.

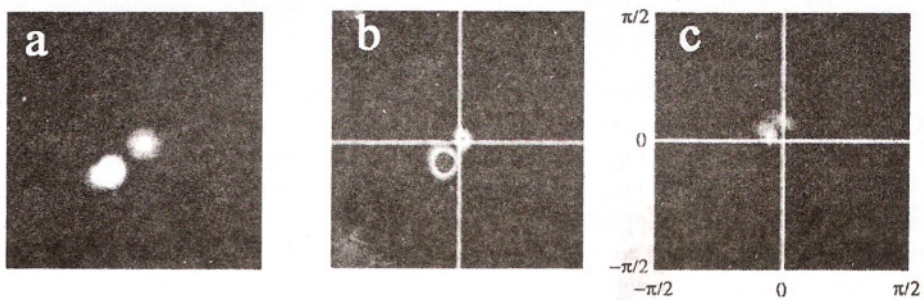

Fig. 2. Gaussian-Gaussian beam interaction: (a) Exit face of the crystal, experimental, (b) The corresponding numerical simulation of the backward beam (at the exit face of the crystal), in the direct space, (c) in the inverse space. Parameters are as in Fig. 1, except for $|F_0|^2 = |B_L|^2 = 7.5$.

3 Comparison between experiment and numerics

The aim of our numerical simulations is to qualitatively capture the most prominent experimental findings, as presented in Refs. [15-17], with the help of a simple theoretical model and a tractable numerical method. To this end we employ an isotropic model without temperature (diffusion) effects. Although the experiment is performed on an anisotropic crystal at a finite temperature, an effort is exerted to minimize the effects of anisotropy and diffusion. Thus, the geometry of beam coupling and the use of incoherent beams

helped reducing the differences between the isotropic and anisotropic interactions in the crystal. Also, an attempt is made in experiment to compensate for the diffusion effects by focusing the backward input beam at the place of exit and in the direction of the output forward beam. The end result is that our numerical simulations closely resemble experimental results concerning the stable CP solitons and single splitup transitions of CP beams, including the size and the direction of transverse displacements. Nonetheless, the experiment still shows the influence of the preferential (c) direction and of the beam bending, which was found to affect the interaction of CP beams [10].

Both the forward and the backward components are found to deflect to the same side. Unstable regions are reached upon increasing the thickness of the crystal and the coupling constant, in both experiment and simulations. In addition, in numerics we also varied the intensity of input laser light. Dynamical behavior in numerical simulations qualitatively follows that of the experimental runs. Typically output beam spots rotate about the input beam positions, or rapidly pass through them, until stable displaced equilibrium positions are found. Then they oscillate about these positions. In case no equilibrium is found, the output beams continue to dance about the input beams indefinitely.

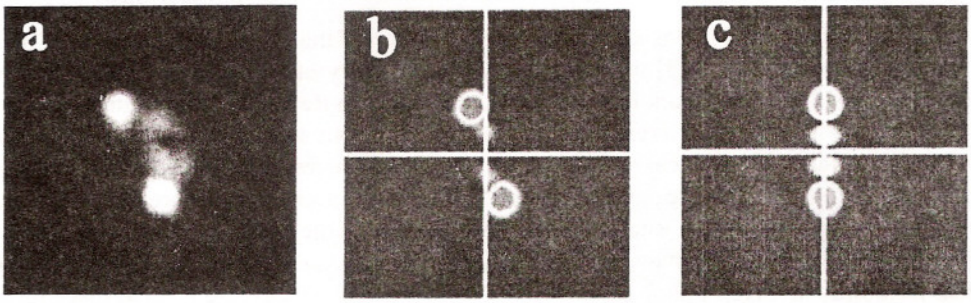

Fig. 3. Dipole-dipole interaction. (a) Experiment, the backward beam at the exit face of the crystal. (b) The corresponding numerical simulation, with an extra noise of 5% added to the input beam intensity. (c) without noise. Parameters are as in Fig. 1, except for $|F_0|^2 = |B_L|^2 = 1.3$. Initial distance between dipole partners is 40 μm.

Concerning the single splitup transition, we observe in our numerical simulations the behavior close to the one in experiment. Hence, in Fig. 1 we present a numerical example only. It is seen that the beams bend, elongate, and split into two. Most of the beam intensity is focused to a new transverse position. The direction of the transverse displacement is approximately in the direction of the external field or the c axis, which is horizontal here. When the coupling constant is increased, the transient dynamics lasts longer, to the point that steady state is not reached over the duration of experiment. The dynamics is such that the exiting beam rotates or rapidly passes through the input beam, or dances irregularly about it. All these dynamical phases could qualitatively be reproduced by numerical simulation (Fig. 2). As it can be seen in Figs. 2(b) and (c), a localized peaked structure in the direct space forms a localized peaked structure in the inverse space, and their dynamics is correlated. In fact, one initially observes a faint ring in the inverse space and then most of the beam intensity focuses to a point.

The next configuration investigated was the dipole-dipole vector CP soliton (Fig. 3). In the case of dipole-dipole CP solitons, two identical dipoles with their components out of phase are counter-propagated head-on. The dipoles are aligned perpendicular to the external field, which always points in the horizontal direction. A transverse splitup occurs again. The direction of the splitup is preferentially along the direction of the external field, and it also depends on the added noise [Fig. 3(b)]. Only in the case when some noise is

added to one of the beams are we able to observe skewed splitups, and achieve better agreement with the experiment. For the case with no noise [Fig. 3(c)], in the beginning we notice oscillations along the y axis, and after a short time these oscillations are damped. Compared to the single CP soliton cases, the cases involving dipoles are more stable and the transient dynamics last shorter.

4 Modulational instability of broad hyper-Gaussian beams

The consideration of broader hyper-Gaussian beams offers rich opportunities for observing complex pattern-forming dynamical behavior [19, 20]. In our case, we also wanted to validate our numerical procedure, by comparing it with the threshold theory of LSA [17]. We found good agreement between numerics and theory in the case of wide hyper-Gaussian beams. Fig. 4 represents the modulational instability of CP hyper-Gaussian beams of FWHM = 150 μm. After a few integration cycles, the rings in the structure appear in direct as well as in inverse space. The structure never reaches a steady state for the duration of the integration. What might be of interest here is that the structure undergoes a series of symmetry breaking changes, starting from an O(2) symmetry at $t = 0$. At $t = 80\ \tau$ a D_4 plane symmetry is reached, after which the final symmetry breaking transition takes place, to C_1. This last transition is apparently the analogue of the splitup transition of CP solitons.

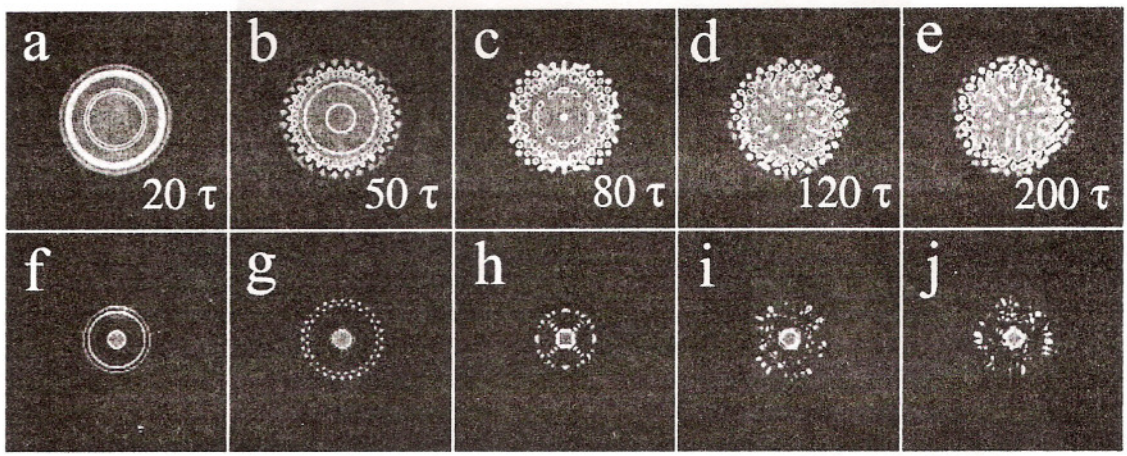

Fig. 4. Modulational instability of a broad hyper-Gaussian beam. The backward component is shown at different times (a)-(e) Direct space, (f)-(j) Inverse space. The order of the hyper-Gaussian is 4, FWHM = 150 μm, other parameters: $\Gamma = 27.6$, $L = 0.5\ L_{fr}$, $|F_0|^2 = |B_1|^2 = 3$.

Fig. 5 presents two further cases of MI, one depicting a steady-rotating hexagonal CP beam structure, and the other an almost stationary transverse pattern of octagonal symmetry. The only difference between the two cases is the width of incident beams, in the first case it equals 100 μm, and in the second 150 μm. All other parameters are the same. The rotating hexagon is interesting in the sense that a quasi-stable symmetric two-ring hexagonal structure breaks its central D_6 symmetry to a C_6 symmetry at about $t = 50\ \tau$, and starts to rotate. This behavior is characteristic of patterns going through a Hopf bifurcation. Also, the beams acquire net angular momentum, which they did not possess to start with. Systems undergoing point symmetry breaking transitions do not conserve angular momentum. An interesting feature in the octagonal pattern is that it also contains octagonal and square patterns of higher order. The mixing and competition of patterns, as well as the appearance of defects and domain-walls, are common features of pattern formation in PR media [19].

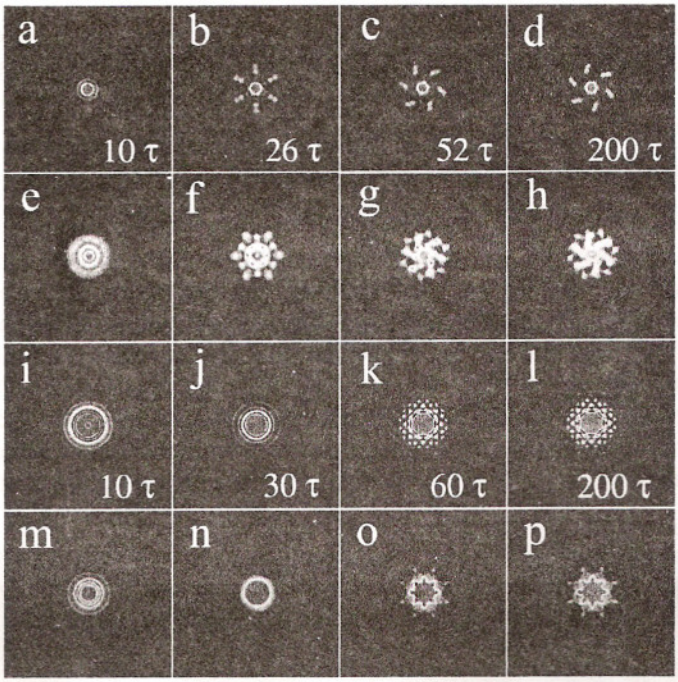

Fig. 5. Modulational instabilities of hyper-Gaussians, resulting in a rotating hexagon (a)-(h), and a steady-state octagonal pattern (i)-(p). The first and third row depict the direct space intensity distributions, the second and fourth row the inverse space distributions. The parameters for both cases are the same, $\Gamma = 16.14$, $L = 3L_D$, $|F_0|^2 = |B_0|^2 = 5$, the only difference being the beam widths: 100 μm in the first, and 150 μm in the second case.

5 Transverse instabilities and stable structures of counter-propagating vortices

Concerning CP vortex beams, a general conclusion of our numerical studies is that the CP vortices in our model can not form stable vortex structures.(i.e. ring-like, with a topological defect) that propagate indefinitely in bulk media [18]. For smaller values of Γ or the propagation distance L we observe stable CP vortices. Nevertheless, they can form very different stable filamented structures in propagating over finite distances, corresponding to the typical photorefractive crystal thicknesses, which are of the order of few L_D. In addition, they can form different stable dynamical structures, such as stable rotating dipoles. It should be noted that in CP geometries, the absolute stability of propagation over indefinite distance is of secondary importance; the influence of both input faces, at any distance, must be felt equally. Hence, stable steady or dynamical structures arising over finite distances are of considerable experimental interest.

Some typical examples of CP vortices seen in our numerics are shown in Fig. 6, which represents the phase diagram in the plane of control parameters. To start with, we consider single head-on input vortices with the same topological charge of +1. For lower values of Γ or L we see stable vortex propagation over the distances of interest (a few L_D). One can notice in the figure a narrow threshold region which separates the stable vortices from other structures. The shape of the threshold region follows the general $\Gamma L = const.$ form we derived earlier for the CP solitons, in our papers [13, 14]. Above this region we see stable dipoles, tripoles and quadrupoles, in the form of standing waves. This is another general feature in our numerical studies: CP vortices with the same topological charge tend to form standing waves, whereas the vortices with the opposite charges tend to form rotating structures. For higher values of the parameters, we identify the following quasi-stable situations: the transformation of a quasi-stable quadrupole into a stable tripole, transformations of quadrupoles into quadrupoles, and a stable rotating dipole. Above the quasi-stable region, CP vortices produce unstable structures, i.e. changing structures of unrecognizable shape.

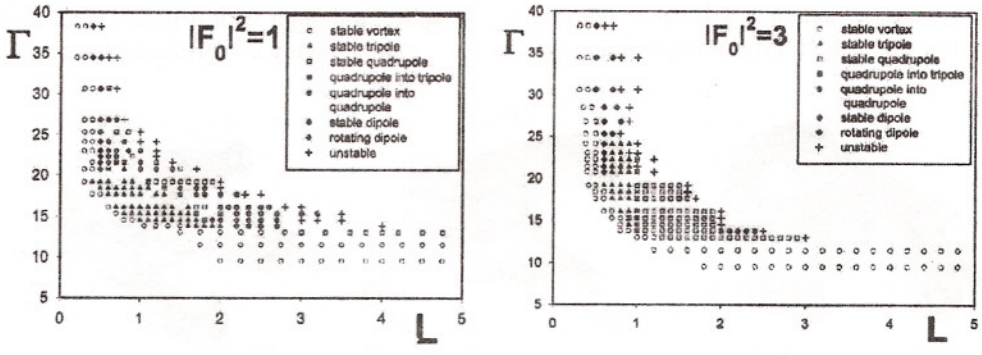

Fig. 6. Typical behavior of CP vortices in the parameter plane. In the two cases shown the input vortices have the same topological charge +1, but different input intensities. Insets list the possible outcomes from vortex collisions.

The most characteristic cases from Fig. 6 are presented in Fig. 7, in the transverse plane. The first, second and fourth columns represent a stable dipole, tripole and quadrupole, respectively. The third and fifth columns present the quasi-stable structures, i.e. the structures that start evolving as one structure, but then transform into another, more stable structure (quadrupole into tripole and quadrupole into quadrupole). The first and second rows correspond to the exit face for the backward beam in the direct and inverse spaces, respectively. The third row shows evolution of the backward beam's total angular momentum, which is normalized to the total beam intensity. As expected, the momentum is steady as long as the beams propagate steady, but starts to vary, in t as well as in z, as soon as the propagation becomes unstable.

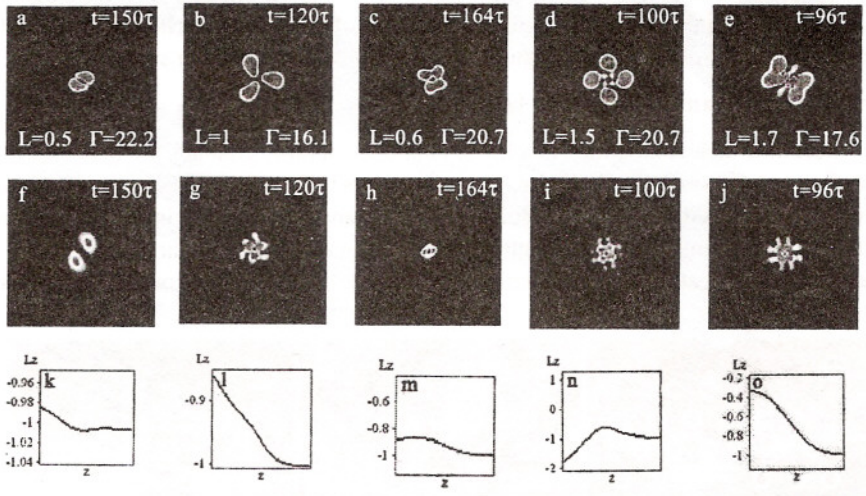

Fig. 7. Stable dipole (first column), the stable tripole (second column), a transformation of an unstable quadrupole into a stable tripole (third column), the stable quadrupole (fourth column) and a transformation of an unstable quadrupole into a stable quadrupole (fifth column). Output face of the backward beam is shown in the direct (a)-(e), and the inverse space (f)-(j). The lower row (k)-(o) presents the corresponding total angular momentum. Parameters Γ and L are given in the figures. The total input intensity of each beam in all cases is 1.

An interesting feature, discerned from Fig. 7, is the beam structure and dynamics in the transverse inverse space. It is seen that in the k space a dipole remains a dipole, a tripole – a tripole (although with

prominent hexagonal features), etc. This is not difficult to understand in terms of the modal decomposition of beams: a Gaussian remains a Gaussian in the inverse space, although with different width and peak intensity. Also, the temporal dynamics and the dynamics in z remain highly correlated in the direct and the

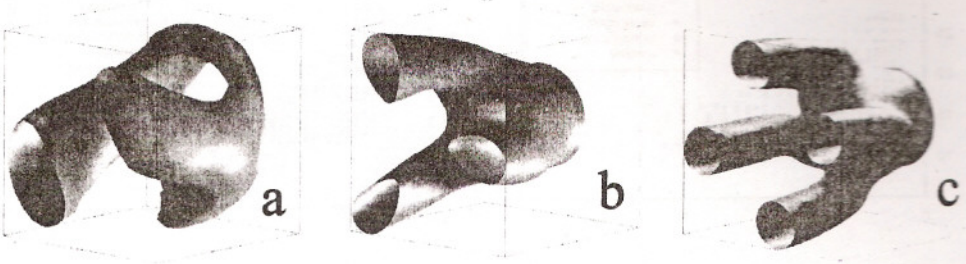

Fig. 8. Standing waves. Isosurface plots of (a) stable dipole, (b) stable tripole and (c) stable quadrupole. The corresponding parameters are as in Fig. 7 (a), (b) and (d), respectively. The isosurfaces at half-maximum intensity are plotted in the direct space, with the transverse plane being vertical and the z axis horizontal.

inverse space. This is the consequence of the assumed model: the optical field is slaved to the slow changes in the space-charge field. The dynamics of beams in both spaces is the image of the dynamics of the E field. However, as it will be seen below, the things considerably change when one considers the propagation of vortex beams in photonic lattices.

Fig. 8 depicts spatial isosurfaces of the stable backward beams presented in Fig. 7, taken at $t/\tau = 200$. They do not change in time. One can clearly see, especially in the case of stable dipole, the spiraling of beam arms along the z axis, which has been described previously in a number of papers treating copropagating vortices and pairs of solitons [3]. The same phenomenon, evidently, appears in the case of CP vortices as well. In general, and especially when the input vortices are of the opposite charge, the resulting structures tend to rotate together [18], owing to the angular momentum inherent in such structures.

6 Counterpropagating beams in photonic lattices

An optical waveguide array embedded in a PR crystal considerably changes the behavior of CP beams, as compared to the wave behavior in bulk media. The continuous O(2) rotational symmetry of the system in the transverse plane is substituted by a discrete point symmetry, and that has bearing on the symmetry-breaking splitup transition. Ours is an axially-invariant photonic crystal, with a planar D_6 symmetry and a central defect, and the axially-propagating beams undergoing symmetry-breaking must comply with the sub-symmetries

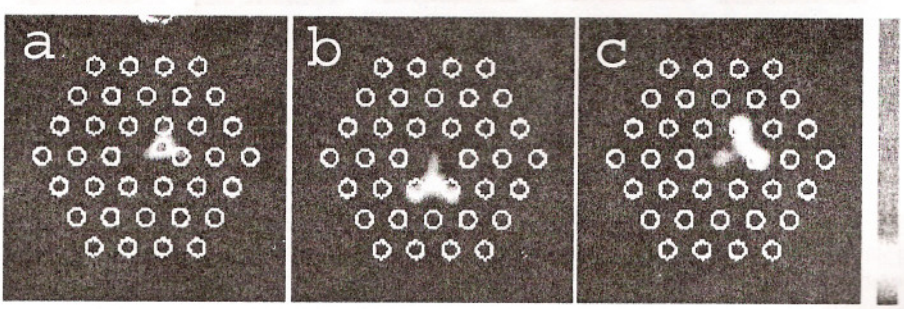

Fig. 9. Intensity distributions of the backward field at its output face in the steady state, for various FWHM of CP input beams: (a) 7 μm, (b) 9 μm, (c) 11 μm Parameters: lattice spacing $d = 28$ μm, FWHM of lattice beams is 9 μm, maximum lattice intensity $I_g = 10I_d$, $\Gamma = 19.3$, $L = 2L_D = 8$ mm, $|F_0|^2 = |B_0|^2 = 10$.

of the plane group. In our case the symmetry breaking usually proceeds along the $D_2 - C_1$ subgroup chain. In addition, the presence of a central defect introduces further differences in the discrete self-focusing, as compared to the infinite lattice, in that the localized optical structures are helped by and pinned to the defect.

A typical example of the splitup symmetry breaking transition in our photonic lattice is presented in Fig. 9. A relatively wide lattice is chosen, lattice spacing 28 μm, with relatively narrow beams of 9 μm. The width of CP components is varied. It is seen that the splitted component of the more narrow CP beam focused in-between the two adjacent lattice sites, whereas that of the wider CP beam focused at the two sites. The same tendency is noted if, instead of the component width, the coupling strength ΓL is increased. Such even and odd discrete solitons are commonplace in periodic arrays of optical waveguides. The choice of the particular pair of adjacent lattice sites among the 6 is incidental, although the direction of polarization of the CP beams is horizontal. The situation is steady-state, however the initial transient behavior lasts longer with the increasing ΓL. Initially the beam jumps transversally, then rotates and oscillates until settling into a steady structure accommodating the lattice's (sub) symmetry. Both CP beams execute the same dynamics, mirror-image of each other.

The splitup transition presented in Fig. 9(c) is shown again in Fig. 10, as a three-dimensional picture along the crystal. It clearly displays the splitup of the forward and backward beams, depicted in green and red, into two beams that focus onto the same two adjacent hexagonal sites on both ends of the crystal. The white rods represent the lattice beams. The green, forward, beam enters from the left, in the middle of the central defect, and the red, backward, beam enters from the right. In the middle of the crystal they cross and split both into two beams that focus onto two adjacent lower lattice sites.

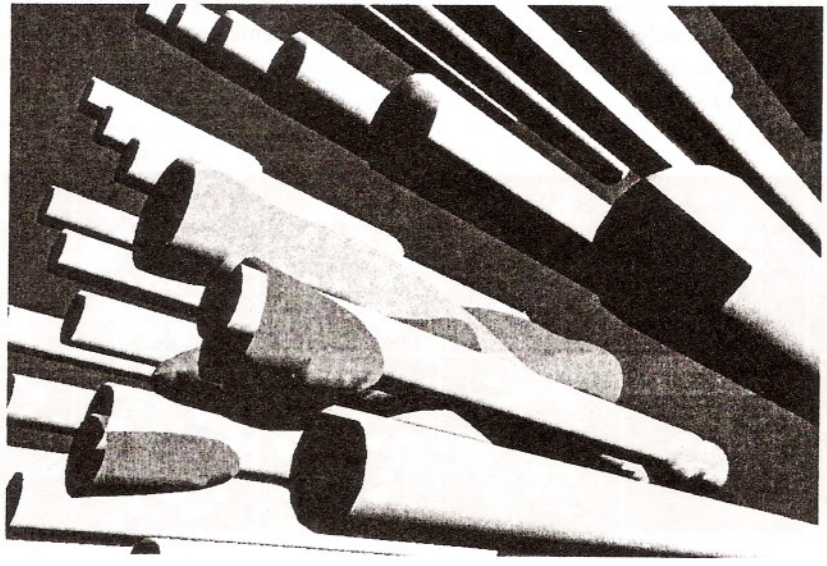

Fig. 10. Isosurface plots at 10% of maximum intensity for the case presented in Fig 9(c): green - forward beam, red - backward beam, white – lattice beams.

Fig. 11 depicts a time-changing, dynamic situation, at different moments, in which narrow centered CP components propagate along the lattice. The parameters are the same as in Fig. 9, except for the width of the CP components, which is 5 μm here. The beam structure is unstable from the beginning, with the three 1D discrete solitonic modes excited initially along the three main symmetry directions. The picture remains centrally-symmetric for awhile, with a clear hexagonal symmetry, but then becomes dynamically broken to

C_1. Thereafter, the beams discretely diffract in asymmetric bursts, at irregular times, along the two of the same 3 symmetry directions. The whole structure slowly rotates counter-clockwise.

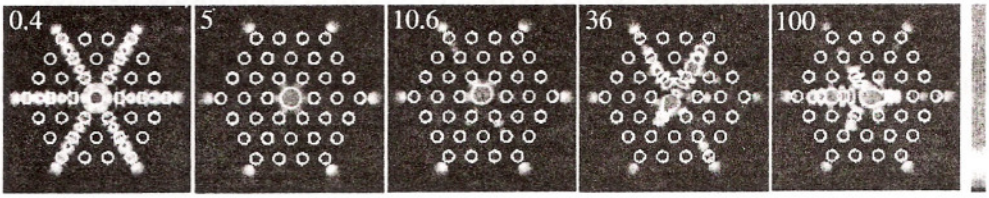

Fig. 11. Dynamics of the backward field of FWHM = 5 μm, at different times. Parameters as Fig. 9.

Fig. 12 represents head-on counterpropagation of two centered vortices, with different topological charges, overlapping with the waveguiding lattice. The values of charges are given in the parenthesis (forward, backward) atop each of the figures, and the width of input vortices is relatively large (26.2 μm). Unlike the case of CP vortices propagating in the absence of lattice, the filamented structures remain steady-state and strongly pinned to the lattice. No rotation of the structures is discerned, either in the case of the same, or of the opposite charges. The angular momentum of CP vortices is transferred to the massive lattice, which remains fixed. The filaments of low-order $(1, \pm 1)$ vortices focus onto the first-order lattice sites, whereas the filaments of higher-order vortices mostly focus in-between the higher-order lattice sites. The size of discrete-diffracted structures increases with the topological charge, however the phase distribution among the filaments reveals the typical vortex linear increase of phase, and branch-cut lines. There is practically no difference between the discrete $(1, \pm 1)$ vortices, and only slight changes in the higher-order vortices. Note the well-preserved vortex at the central defect of the $(1, \pm 1)$ structure. Stable elementary vortices could not be observed in the case without lattice, at such high values of the coupling strength ΓL. The plane symmetry of all these structures is C_6.

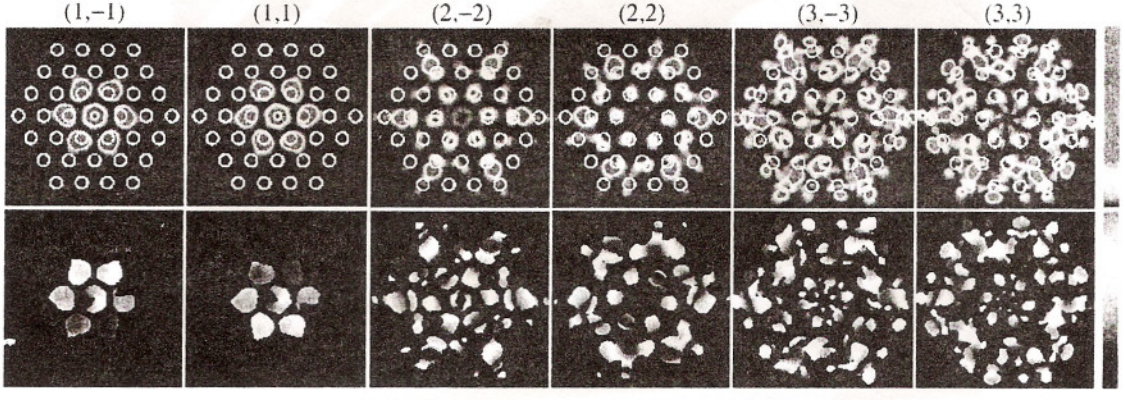

Fig. 12. Intensity (upper row) and phase (lower row) distributions of the backward field at its output face in the steady state, for different topological charges, recorded on the top of each figure. Parameters are as in Fig 9, input FWHM of vortices is 26.2 μm.

7 Conclusions

In summary, we report on the various aspects of counterpropagation of self-trapped beams in isotropic local saturable photorefractive media, including the presence of an optically-induced photonic lattice. We present some experimental data on the three-dimensional counterpropagating spatial vector solitons and on

the dipole-dipole interacting beams. A peculiar dynamic behavior of CP solitons is observed, in that the counterpropagating components suddenly change their transverse positions, and from an attracting interaction switch to repelling. Previously stable equilibrium becomes a limit cycle, the behavior characteristic of a Hopf bifurcation happening in the system. Utilizing a simple model we explain this behavior as a spontaneous symmetry-breaking first-order phase transition. We also observe rich dynamics of the three-dimensional counterpropagating solitons and vortices, and formulate a theory capable of capturing such dynamics. We obtain good agreement between the numerical simulations and experimental results. A few examples of the standard MI of broad CP beams are also presented, in order to validate our numerical algorithm and verify our results concerning the threshold behavior. Finally, we display the axial counter-propagation of solitonic beams and vortices in an optical lattice with a central waveguiding defect. Although sharing some common features with the counterpropagation in the absence of lattice, such as the splitup transition, the discrete diffraction brings novel moments into the picture, such as the appearance of discrete solitons, the discrete symmetry breaking, and pinning to the central defect. In the case of CP vortices one also observes strong pinning to the lattice, improved stability of the central basic vortex, and the absence of clear rotation of vortex filaments.

Acknowledgements

Work at the Institute of Physics is supported by the Ministry of Science and Environment Protection of the Republic of Serbia, under the project OI 1475.

References

1 Trillo S, Torruellas W, eds., *Spatial Solitons* (Springer, New York) 2001.

2 Segev M, ed., *Special Issue on solitons, Opt Phot News,* 13 (2002) No. 2.

3 Kivshar Y S, Agrawal G P, *Optical Solitons* (Academic Press, San Diego) 2003.

4 Desyatnikov A S, Torner L, Kivshar Y S, *Prog Optics,* 47 (2005) 219.

5 Neshev D, Alexander T J, Ostrovskaya E A, Kivshar Y S, Martin H, Makasyuk I, Chen Z, *Phys Rev Lett,* 92 (2004) 123903; Chen Z, Martin H, Bezryadina A, Neshev D, Kivshar Y S, Christoulides D N, *J Opt Soc Am,* B 22 (2005) 1395.

6 Ferrando A, Zacares M, Fernandez P, Binosi D, Monsoriu J A, *Opt Express* 11 (2003) 452; *Opt Express,* 12 (2004) 817.

7 Haelterman M, Sheppard A P, Snyder A W, *Opt Commun,* 103 (1993) 145.

8 Cohen O, Uzdin R, Carmon T, Fleischer J W, Segev M, Odulov S, *Phys Rev Lett,* 89 (2002) 133901.

9 Cohen O, Carmon T, Segev M, Odoulov S, *Opt Lett,* 27 (2002) 2031.

10 Cohen O, Lan S, Carmon T, *Opt Lett,* 27 (2002) 2013.

11 Rotschild C, Cohen O, Manela O, Carmon T, Segev M, *J Opt Soc Am,* B 21 (2004) 1354.

12 Belic' M, Jander Ph, Strinic A, Desyatnikov A, Denz C, *Phys Rev,* E 68 (2003) 025601.

13 Motzek K, Jander Ph, Desyatnikov A, Belic M, Denz C, Kaiser F, *Phys Rev,* E 68 (2003) 066611.

14 Belic M, Petrovic M, Jovic D, Strinic A, Arsenovic D, Motzek K, Kaiser F, Jander Ph, Denz C, Tlidi M, Mandel P, *Opt Express,* 12 (2004) 708.

15 Jander Ph, Schröder J, Denz C, Petrovic M, Belic M, *Opt Lett* 30 (2005) 750; Schröder J, Jander Ph, Denz C, Richter T, Motzek K, Kaiser F, *Opt Lett,* 30 (2005) 1042.

16 Petrovic M, Jovic D, Belic M, Schröder J, Jander Ph, Denz C, *Phys Rev Lett,* 95 (2005) 053901.

17 Petrovic M, Jovic D, Belic M, Schröder J, Jander Ph, Denz C, *Opt Express,* 13 (2005) 10717.

18 Jovic D, Arsenovic D, Strinic A, Belic M, Petrovic M, *Opt Express,*13 4382 (2005).

19 Denz C, Schwab M, Weilnau C, *Transverse pattern formation in photorefractive optics* (Springer, Berlin) 2003.

20 Sandfuchs O, Kaiser F, Belic M, *Phys Rev,* A 64 (2001) 063809.

[*Received* : 11.11.2005]